The Astronomical Journal, 152:79 (4pp), 2016 October doi:10.3847/0004-6256/152/4/79

THE ALBEDO DISTRIBUTION OF NEAR EARTH ASTEROIDS

Edward L. Wright[1], Amy Mainzer[2], Joseph Masiero[2], Tommy Grav[3], and James Bauer[2,4]
[1] UCLA Astronomy, P.O. Box 951547, Los Angeles, CA 90095-1547, USA; wright@astro.ucla.edu
[2] Jet Propulsion Laboratory, California Institute of Technology, 4800 Oak Grove Drive Pasadena, CA, 91109-8001, USA
[3] Planetary Sciences Institute, 1700 E Fort Lowell Road #106, Tucson, AZ 85719, USA
[4] Infrared Processing and Analysis Center, 770 South Wilson Avenue Pasadena, CA 91125, USA
Received 2016 May 6; revised 2016 June 22; accepted 2016 June 23; published 2016 September 9

ABSTRACT

The cryogenic *Wide-field Infrared Survey Explorer* (*WISE*) mission in 2010 was extremely sensitive to asteroids and not biased against detecting dark objects. The albedos of 428 near Earth asteroids (NEAs) observed by *WISE* during its fully cryogenic mission can be fit quite well by a three parameter function that is the sum of two Rayleigh distributions. The Rayleigh distribution is zero for negative values, and follows $f(x) = x\exp[-x^2/(2\sigma^2)]/\sigma^2$ for positive x. The peak value is at $x = \sigma$, so the position and width are tied together. The three parameters are the fraction of the objects in the dark population, the position of the dark peak, and the position of the brighter peak. We find that 25.3% of the NEAs observed by *WISE* are in a very dark population peaking at $p_V = 0.030$, while the other 74.7% of the NEAs seen by *WISE* are in a moderately dark population peaking at $p_V = 0.168$. A consequence of this bimodal distribution is that the congressional mandate to find 90% of all NEAs larger than 140 m diameter cannot be satisfied by surveying to $H = 22$ mag, since a 140 m diameter asteroid at the very dark peak has $H = 23.7$ mag, and more than 10% of NEAs are darker than $p_V = 0.03$.

Key words: minor planets, asteroids: general

1. INTRODUCTION

The *Wide-field Infrared Survey Explorer* (*WISE;* Wright et al. 2010) mapped the entire sky between 2010 January 14 and July 17, then continued on to map the entire sky again prior to 2011 February 1. On 2010 August 7, the outer cryogen tank ran out of solid hydrogen coolant, ending the 4 band cryogenic phase of the *WISE* mission. The NEOWISE mission is a separately funded program to search for near Earth objects (NEOs) in the *WISE* data. NEOs include both asteroids and comets. In this paper, we will only consider NEAs, and we study the sample of 428 NEAs observed with all 4 *WISE* bands during 2010 (Mainzer et al. 2011). The wide range of wavelengths spanning the peak of the thermal infrared emission allows the near Earth asteroid thermal model (NEATM, Harris 1998) to work very well, since the 4.6, 12, and 22 μm fluxes are all dominated by thermal emission for NEAs and their ratios provide a tight constraint on the beaming parameter η, while the 22 μm flux gives a diameter that is only weakly dependent on η. This NEOWISE sample of NEAs with radiometric diameters is more than an order of magnitude larger than the sample of 36 objects studied by Stuart & Binzel (2004). We find in this paper that a simple three parameter model provides a very useful approximation to the observed distribution of albedos.

Masiero et al. (2011) found bimodal albedo distributions for the the inner, middle, and outer main belt asteroid populations with different dark fractions as a function of distance from the Sun. The optical colors of asteroids are known to correlate with the albedo, with the higher albedo S ("stony") type being redder than the lower albedo C ("carbonaceous") type (Bowell & Lumme 1979, pp. 132–169). Thus the albedo distribution of the NEAs could give clues about the source or sources of the NEA population. Indeed, Granvik et al. (2016) find that the high albedo and low albedo fractions of the NEOWISE NEA sample have significantly different parent distributions, confirming a result from Mainzer et al. (2012). They also find that there are fewer observed NEAs with small perihelia than are predicted by their models, and suggest that the low perihelion ($q < 0.2$ au) objects have been thermally disrupted, based on a large sample of NEAs from the Catalina Sky Survey. They suggest that the darker objects are more subject to disruption by thermal stress when close to the Sun, but there are only five low perihelion ($q < 0.2$ au) NEAs in the NEOWISE sample, so this last suggestion requires a larger sample of NEA albedos for verification.

The NEA albedo distribution also enters into estimates of the hazard due to Earth impacts. In 2005, Congress gave NASA the goal of finding 90% of all near Earth objects larger than 140 m in diameter.[5] One use of the albedo distribution proposed here is to determine what optical limiting magnitude is needed to meet this objective. The optical absolute magnitude is given by $H = 5\log([1329\text{ km}]/D) - 2.5\log(p_V)$ (Bowell et al. 1989, pp. 524–556), and the usual assumption that $H = 22$ mag corresponds to $D = 140$ m requires that $p_V = 0.142$. However, since p_V is distributed over a wide range of values, the actual optical limiting magnitude needed to satisfy the mandate depends on the size distribution of NEAs, with shallower slopes leading to somewhat relaxed search limits.

2. OBSERVATIONS

The data set used is the collection of 428 NEAs observed by *WISE* during the fully cryogenic phase of the mission: the seven months from 2010 January 7 to August 7. This is the same data used by Mainzer et al. (2011). Of the 428 NEAs in the data set, 9 have only *WISE* observations with no optical followup. These objects have an unknown albedo and are not used in the fit. They are perhaps preferentially low albedo objects, but this is only a potential 2% bias in the abundance of dark objects. However, these objects have fairly long arcs in the

[5] The National Aeronautics and Space Administration Authorization Act of 2005 (Public Law 109-155), 2005 January 4, Section 321, George E. Brown, Jr. Near-Earth Object Survey Act.

WISE data. Many other *WISE* tracklets are shorter arcs, and if these receive no optical followup, they are filed by the Minor Planet Center (MPC) without an orbit. Mainzer et al. (2011) noted that during the four band fully cryogenic portion of the NEOWISE mission, about 15–20 NEO candidates appeared on the MPC NEO Confirmation Page but received no followup.

Thus, while using infrared observations eliminates the discovery bias against dark objects, there can still be a followup bias against dark objects. An example is 2015 SS_{20}, which was on the MPC NEO Confirmation Page for two weeks without receiving any optical followup. It was designated 2015 SS_{20} and filed without an orbit. Searching the NEOWISE image data for 3σ bumps led to a tentative longer observational arc, which led to a very faint counterpart on previously obtained CHFT MegaCam frames (Forshay et al. 2015), and then to a cross identification with 2015 WL_{16}, another NEOWISE tracklet that was also designated without followup or an orbit. IR fits to the NEOWISE data show that the diameter is definitely larger than 140 m, but the H magnitude is 22.7 in Forshay et al. (2015). While it is tempting to assume that the low albedo of this object led to the lack of followup, it is quite likely that the phase of the moon, which was waxing gibbous at the discovery 2015 SS_{20} and full at the discovery of 2015 WL_{16} had a large effect as well. We have used this example to inform our assumption about the nature of the nine objects that have only *WISE* observations. Three of these objects were discovered in a three day interval just before the full Moon in 2010 June. Another three were discovered at extreme southern declinations $\delta < -72°$, where followup opportunities were limited. As a result, we have assumed that these nine objects were missed for reasons other than a very low albedo, and have not made any correction to the dark fraction derived from the 419 objects that were followed up by optical observers.

3. PREVIOUS FITS

Mainzer et al. (2011) used a five parameter double Gaussian to fit the NEA albedo distribution:

$$p_{2G}(p_V) = f \exp\left(-\frac{(p_V - d)^2}{2e^2}\right) + c \exp\left(-\frac{(p_V - b)^2}{2a^2}\right). \quad (1)$$

While this appears to have six parameters, one of the degrees of freedom is taken away by the normalization constraint, $\int p(p_V) dp_V = 1$. The dark albedo peak was found to be $d = 3.4\%$, while the bright albedo peak was found to be $b = 15.1\%$. This two Gaussian model for the albedo distribution has the conceptual problem that it predicts a non-zero probability density for small negative albedos, while the albedo is actually constrained to be non-negative. This is easily solved by replacing the non-zero density by zero. A related problem is that the two Gaussian model overpredicts the abundance of very low albedos, because the probability density does not go to zero as the albedo goes to zero.

Note that the dark Gaussian accounts for 28.8% of the cumulative probability in this two Gaussian model.

4. RAYLEIGH DISTRIBUTION FITS

Problems with the two Gaussian model can be fixed by replacing the Gaussian with a Rayleigh distribution. The Rayleigh distribution is the distribution of the radius in a two-dimensional Gaussian. It is clearly zero for negative values, because the radius is always non-negative. The probability density goes to zero as the radius goes to zero. The full formula for a Rayleigh distribution is

$$p(x) = \frac{x \exp(-x^2/2\sigma^2)}{\sigma^2}. \quad (2)$$

The mean of x is $\langle x \rangle = \sigma\sqrt{\pi/2}$, and the fractional width of the distribution is $\sqrt{\mathrm{var}(x)}/\langle x \rangle = 0.5227$. This ratio can be compared to $d/e = 0.41$ and $b/a = 0.81$ in the two Gaussian model of Equation (1). The peak of $p(x)$ occurs at σ, but the most likely value of $\ln(x)$ occurs at $\sigma\sqrt{2}$.

The bimodality of the albedo distribution requires that the full model includes two Rayleigh distributions, giving the formula

$$p_{2R}(p_V) = f_D \frac{p_V e^{-p_V^2/2d^2}}{d^2} + (1 - f_D) \frac{p_V e^{-p_V^2/2b^2}}{b^2}. \quad (3)$$

This is an example of a finite mixture model in statistics (McLachlan & Peel 2000) and the particular case of two Rayleigh distributions has been used in a very different application to failure time distributions by Attia (1993).

The three parameters in Equation (3) were adjusted to minimize the maximum deviation between the observed and model cumulative distribution functions. This corresponds to minimizing the Kolmogorov–Smirnov statistic. The motivation for using this criterion to optimize the parameters comes from the congressional goal: we want to have a model that is very close to reality at the 10th percentile of the distribution in order to be sure to find 90% of all NEAs bigger than 140 m diameter. The resulting parameters are the dark fraction $f_D = 0.253$, the dark peak $d = 0.030$, and the bright peak $b = 0.168$. The best fit $p(p_V)$ is shown in Figure 1. The goodness of fit is shown in Figures 2 and 3.

The best fit has a maximum deviation between the model and observed CDFs of $\Delta = 0.027$. If we had not adjusted the three parameters for a best fit, the probability of a deviation larger than this due to chance fluctuations alone in the Kolmogorov–Smirnov test would be 92%. However, adjusting parameters to minimize Δ has a strong effect on the probabilities. To evaluate this effect, we generated random data sets using the best-fit model and the methods in Section 7,

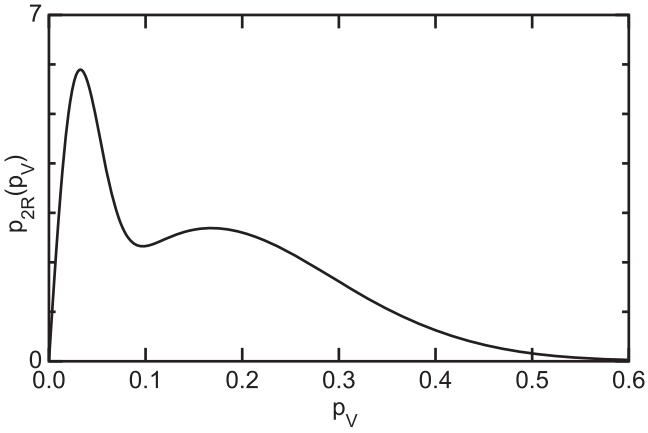

Figure 1. Two Rayleigh distribution model for the probability density function of near Earth asteroid albedos.

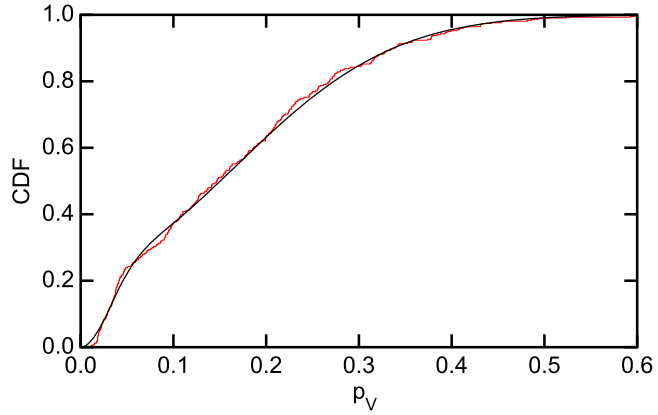

Figure 2. Comparison of the cumulative distribution function (CDF) for the observed set of NEAs (red staircase function) with the CDF for the two Rayleigh distribution model.

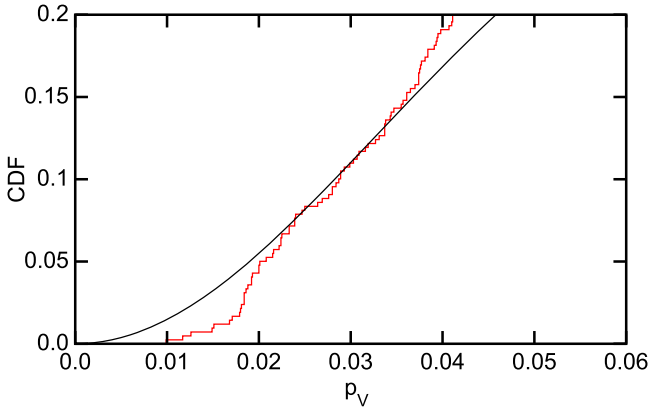

Figure 3. Low albedo corner of Figure 2.

and then readjusted the three parameters for a best fit to each random data set. We got better fits with lower Δ than the observed data for 96% of the random data sets. Thus the two Rayleigh distribution model is a convenient and acceptable fit, not ruled out by the current data, but should not be taken as a final description of the albedo distribution. The scatter in the parameters for the fits to the random data sets were $\sigma(f_D) = 0.032$, $\sigma(d) = 0.003$, and $\sigma(b) = 0.006$. The dark fraction is determined to a relative accuracy of 13% by the NEOWISE data set and the dark albedo peak is determined to a relative accuracy of 10%.

5. MAIN BELT ALBEDO DISTRIBUTION

Masiero et al. (2011) fit mixture models with two log normal distributions to the main belt asteroid albedos derived from NEATM fits to the *WISE* four-band data. This data set contains over 10^5 objects. Thus Masiero et al. (2011) were able to subdivide the data set into inner, middle, and outer main belt samples, and fit for a five parameter dual log normal distribution in each subsample.

The three main belt albedo distributions all have a dark albedo peak at $p_V = 0.06$ with a width shown by $\sigma_+ = 0.03$ and $\sigma_- = 0.02$. Thus the σ in the logarithm was $\ln(1.5) = 0.41$. The most likely logarithm of p_V in the dark peak of the two Rayleigh distribution in Equation (3) occurs at $b\sqrt{2} = 0.042$ compared to 0.06 in the main belt, so the NEA albedo distribution has a darker and wider dark peak than the main belt distributions. The fraction of objects in the dark peak was 47% to 73%, so the MBA albedo distributions in Masiero et al. (2011) have a larger fraction of dark asteroids than the NEA distribution.

6. CUMULATIVE DETECTION LIMITS

The albedo distribution derived here has 90% of NEAs with $p_V > 0.03$. Thus if one wants to find 90% of all 140 m sized NEAs, then one must search down to $H = 23.7$. However, the congressional mandate is to find 90% of all NEAs 140 m or larger, and finding the necessary H mag limit for this criterion depends on the size distribution of NEAs. For example, if the size distribution is very shallow, most of the objects larger than 140 m in diameter will be much larger than 140 m and thus easier to find. In this paper, we will use $N(>D) \propto D^{-1.3}$ which is the slope found by Ivezic et al. (2002) for main belt asteroids with $D < 5$ km using the Sloan Digital Sky Survey. The slope also agrees with $N(>D) \propto D^{-1.32\pm0.14}$ found for NEAs between 100 m and 1 km by Mainzer et al. (2011). The probability density for H magnitudes for a given size distribution $p(D)$ with $D > D_m$ and albedo distribution $p(p_V)$ is

$$p(H) = \int_{D_m}^{\infty} \int_0^{\infty} \delta\left(H - 5\log\left(\frac{1329\ \mathrm{km}}{D\sqrt{p_V}}\right)\right) \times p(p_V)dp_V p(D)dD \quad (4)$$

when we assume that the albedo and size are independent, since Mainzer et al. (2011) did not see a correlation of albedo and size. Note that geometric albedos like p_V can be larger than 1 if the phase function is sharply peaked: Scotchlite® tape is an example. However, in any case, these high values of p_V contribute little to the integral. For any D, the value of p_V that gives H is

$$p_V = \left(\frac{1329\ \mathrm{km}}{D}\right)^2 10^{-0.4H}. \quad (5)$$

The derivative dp_V/dH needed to evaluate Equation (4) is given by $dp_V = -(0.4\ln 10)p_V dH$. Inserting these values for p_V and dp_V into Equation (4) gives

$$p(H) = (0.4\ln 10)\int_{D_m}^{\infty} p_{2R}(p_V)p_V p(D)dD \quad (6)$$

which is plotted in Figure 4. The vertical black line in this figure is at $H = 22.84$ mag, and the area to the right of this line is 90% of the total. So an optical survey that is 100% complete for $H < 22.84$ will detect 90% of all asteroids larger than 140 m diameter for $N(>D) \propto D^{-1.3}$. Similar limits for the main belt albedo distributions in Masiero et al. (2011) are $H < 22.5$, <22.6, and <22.8 mag for the inner, middle, and outer main belt subsamples.

However, 100% completeness is not realistic. The red curve in Figure 4 shows $p(H)$ multiplied by a completeness function that is 90% for $H = 23$ mag and with the incompleteness scaling inversely with the flux, or $0.1 \times 10^{0.4(H-23)}$. Thus the completeness is 96% at $H = 22$ and 99% at $H = 20.5$. The red vertical line is at $H = 23$ mag, and the area to the right of this line contains 90% of all the asteroids with diameters greater than 140 m.

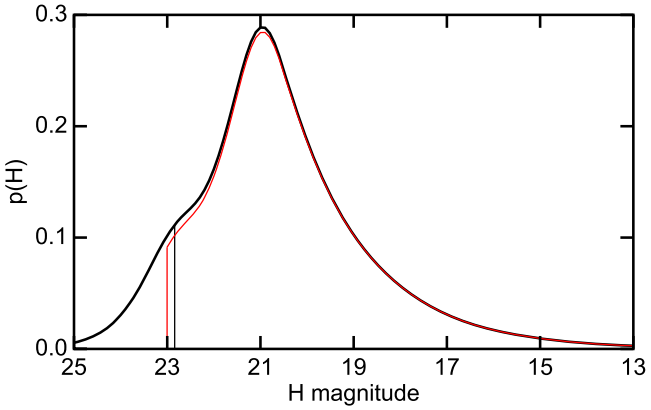

Figure 4. Thick curve shows the distribution of H magnitudes for asteroids with diameters greater than 140 m and $N(>D) \propto D^{-1.3}$. The thin red curve shows this $p(H)$ multiplied by a simple survey completeness model with 90% completeness at $H = 23$ mag and 96% completeness at $H = 22$ mag. 90% of the $D > 140$ m asteroid population is contained in the area under the thin red curve to the right of vertical red line at $H = 23$. A survey that is 100% complete for H brighter than the thin vertical black line at $H = 22.84$ mag will also find 90% of objects bigger that 140 m.

The distribution of H in Figure 4 is very similar to Figure 6 of Grav et al. (2016), who used Monte Carlo methods with albedos chosen randomly from the actual list of albedos in Mainzer et al. (2011). Thus the conclusion that optical surveys should strive for completeness down to $H = 23$ mag is not affected by the details of the fit.

7. USEFUL APPLICATIONS

One potential use for the albedo distribution shown here is in simulations of surveys. For this, one needs to randomly choose p_V from the distribution in Equation (3). This is easily accomplished using two independent random variates x and y drawn from a uniform distribution over [0, 1). The procedure takes $t = d$ if $x < f_D$ or $t = b$ otherwise, and then $p_V = t\sqrt{-2\ln(1-y)}$.

A second use for Equation (3) is as a Bayesian prior on the albedo when fitting for the diameter of an NEA based on limited infrared data that are only 3.4 μm and 4.6 μm. This allows reasonable corrections for the effects of scattered sunlight on the 3.4 μm flux of an NEA even if no optical data are available. With no optical data, a higher albedo means less of the 3.4 μm flux is thermal, so the asteroid must be cooler, leading to a higher η and a larger diameter. This variation of diameter with albedo is smaller than the $D \propto {p_V}^{-0.5}$ when only optical data are available, and it has the opposite sense. For example, if an NEA 1.155 au from the Sun with $\eta = 1$, emissivity $\epsilon = 0.9$, albedo $p = 0.168$ and slope parameter $G = 0.15$ is observed at a 60° phase angle, but is analyzed assuming an albedo $p = 0.03$, the NEATM derived diameter based on 3.4 and 4.6 μm data alone goes down by a factor of 0.83, while the diameter derived from optical data alone goes up by a factor of $\sqrt{0.168/0.03} = 2.37$. This degeneracy between albedo and diameter in optical-only or infrared-only cases can be constrained by using an informative prior on the albedo. A Monte Carlo Markov Chain, using Equation (3) as a prior, can give a good picture of the resulting diameter uncertainty that allows for the non-Gaussianity of the albedo distribution. This prior can be implemented by using a uniform prior on $\ln(p_V)$ and applying a penalty to χ^2 of $-2\ln[p_V p_{2R}(p_V)]$.

8. CONCLUSIONS

The distribution of albedos for near Earth asteroids is very broad, and it can be written as the sum of two Rayleigh distributions with peaks that differ by a factor close to six in albedo. The existence of the dark peak in the albedo distribution is very well established by the NEOWISE data set, with a confidence of 8σ. As a result, the congressional goal to find 90% of all NEAs larger than 140 m diameter cannot be met by surveying to a limit of $H < 22$ mag. Optical surveys must aim for very substantial completeness down to $H = 23$ mag to satisfy the mandate.

This publication makes use of data products from the *Wide-field Infrared Survey Explorer*, which is a joint project of the University of California, Los Angeles, and the Jet Propulsion Laboratory/California Institute of Technology, funded by the National Aeronautics and Space Administration.

The *WISE* data were all provided by the Infrared Science Archive at Caltech.

Facility: WISE.

REFERENCES

Attia, A. 1993, Microelectrnoics Reliablity, 33, 859
Bowell, E., Hapke, B., Domingue, D., et al. 1989, in Asteroids II, ed. R. P. Binzel, T. Gehrels, & M. S. Matthews (Tucson, AZ: Univ. Arizona Press), 524
Bowell, E., & Lumme, K. 1979, in Colorimetry and Magnitudes of Asteroids, ed. T. Gehrels (Tucson, AZ: Univ. Arizona Press)
Forshay, P., Wells, L., Tholen, D. J., & Williams, G. V. 2015, MPEC, K15Y56
Granvik, M., Morbidelli, A., Jedicke, R., et al. 2016, Natur, 530, 303
Grav, T., Mainzer, A. K., & Spahr, T. 2016, AJ, 151, 172
Harris, A. W. 1998, Icar, 131, 291
Ivezic, Z., Juric, M., Lupton, R. H., Tabachnik, S., & Quinn, T. 2002, Proc. SPIE, 4836, 98
Mainzer, A., Grav, T., Bauer, J., et al. 2011, ApJ, 743, 156
Mainzer, A., Grav, T., Masiero, J., et al. 2012, ApJ, 752, 110
Masiero, J. R., Mainzer, A. K., Grav, T., et al. 2011, ApJ, 741, 68
McLachlan, G., & Peel, D. 2000, Finite Mixture Models (New York: Wiley-Interscience)
Stuart, J. S., & Binzel, R. P. 2004, Icar, 170, 295
Wright, E. L., Eisenhardt, P. R. M., Mainzer, A. K., et al. 2010, AJ, 140, 1868